Physical and electrical characteristics of EDM debris

J.W. Murray [a], J. Sun [b], D.V. Patil [b], T.A. Wood [c], A.T. Clare [a],*

[a] Department of M3, Institute for Advanced Manufacturing, Faculty of Engineering, University of Nottingham, Nottingham, NG7 2RD, UK
[b] School of Engineering, University of Edinburgh, King's Buildings, Mayfield Road, Edinburgh EH9 3JL, UK
[c] School of Physics and Astronomy, University of Edinburgh, King's Buildings, Mayfield Road, Edinburgh EH9 3JL, UK

ARTICLE INFO

ABSTRACT

In EDM, debris plays a key role in the electrical conditions of the discharge gap prior to each spark. Despite this, analysis of debris at all length-scales has not yet been performed, and therefore the nature of debris produced by electrical discharge processes is not fully understood. In this study debris created by the machining of two electrode materials set as negative polarity, silicon and titanium carbide, was centrifuged and imaged using SEM and TEM. From this analysis it was shown that electrode debris is 1 nm or lower and up to 10 μm in size. Population analysis of the particle size distribution was used to inform an electric field model based on a lattice Boltzmann method framework, simulating the effect of the presence of such debris on the electric field strength. This method is shown to be able to capture the local variation of the electric field and predict qualitatively the correct trend of the electric field strength increasing against the debris concentration. Such data is important for prediction and control of discharge gap size, as well as understanding the impact of a build-up of debris on uncontrolled sparking.

1. Introduction

In electrical discharge machining (EDM), sparks occur at a frequency on the order of 10,000/s or greater. In order to yield a good surface finish, a randomised spark location is desired, which results in discharge craters evenly distributed on the workpiece. On the other hand, repeated sparking in the same location can result in cavitation in the workpiece and excessive electrode wear (Tosello et al., 2008), and due to difficulty in flushing in such locations, can cause the subsequent build-up of machined debris in this region, resulting in further non-randomised and uncontrolled sparking, referred to as arcing. A small amount of excessive sparking in one region can lead to a low level of cavitation. The presence of this small cavity can cause debris to be trapped, further exacerbating localised sparking and again increasing the size of the cavity.

The probability of discharge is determined by the ease of electrical breakdown within the spark gap. The electrical breakdown strength at any point between the two electrodes is influenced by the presence of debris. Because of this, under normal machining conditions, flushing is applied to the machining gap in order to remove this material to maintain consistent electrical condi-

tions. Despite this, Luo (1997) showed that the presence of debris particles in the gap in fact plays a necessary role in yielding stable machining conditions by improving the distribution of spark location, and that a too pure dielectric can promote uncontrolled sparking.

Deliberate addition of conductive debris into the machining gap has also been explored for enhancing the machining process, as well as for electrical discharge coating. For example addition of extra powder to the machining gap has been used to increase the material removal rate as well as improve surface finish. Kansal et al. (2007) showed that an improved machining rate was achieved using Silicon power added at a concentration of 4 g/l. Chow et al. (2008) demonstrated that both improved material removal rate and better surface finish was achieved with the addition of SiC powder to a water dielectric. The improved material removal rate is explained by the increased discharge gap and better distribution of discharges, leading to reduced "servo hunting", resulting in more efficient machining. Improved surface finish has been observed by many researchers when using additional powder in the machining gap, and it may be explained by the widening of the discharge gap resulting in a lower discharge energy density and lower plasma pressure, resulting in shallower craters and a smoother surface finish (Peças and Henriques, 2003). Chow et al. (2008) also explained that a reduced discharge energy density may be caused by the division of sparks into two or more individual sparks one after the other during one discharge on-time, thereby

* Corresponding author. Fax: +44 1159513800.
E-mail addresses: james.murray@nottingham.ac.uk (J.W. Murray), j.sun@ed.ac.uk (J. Sun), Dhiraj.Patil@ed.ac.uk (D.V. Patil), tiffany.wood@ed.ac.uk (T.A. Wood), adam.clare@nottingham.ac.uk (A.T. Clare).
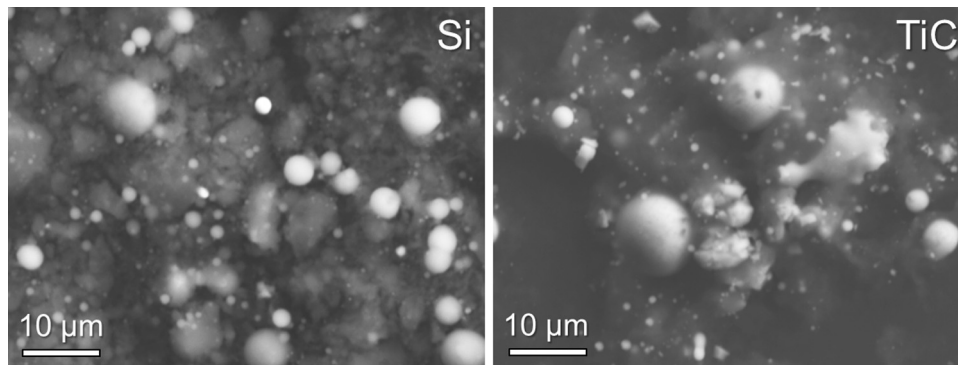
Fig. 1. Back-scattered SEM images of Si machined at 5.5 A and TiC debris machined at 10 A.

dividing the total energy transferred to the workpiece between several discharge spots, reducing the size of resulting discharge craters, thereby improving surface finish. Voltage and current waveforms confirmed this.

Debris also plays a key role in electrical discharge coating (EDC). In EDC, a coating is produced on a workpiece surface normally of positive polarity. The coating material is either deliberately added as a powder to the dielectric, or the opposite electrode is used as a donor electrode, which sheds material to the discharge gap and is subsequently deposited gradually as a coating by each discharge. In both cases, debris must be present in the machining gap and therefore its physical characteristics and influence on electrical conditions should be fully understood.

The presence of debris has a strong effect on the electrical breakdown strength of the discharge gap, however, no theoretical model of the gap is available which considers the particle sizes and characteristics of debris produced during actual EDM. A comprehensive microscopic analysis of debris formed during EDM, including high resolution analysis for example using TEM to study all scales of EDM debris, has also not been performed. Gatto et al. (2013) performed image processing of debris particles which were collected by a filtration system after EDM, although smaller particles have not been collected. In their work however, a focused ion beam (FIB) was used to cross-section some particles, interestingly revealing a partially hollow structure. Murti and Philip (1987) also analysed the size, shape and distribution of debris particles in normal EDM and ultrasonic-assisted EDM in which the workpiece is vibrated. Based on SEM imaging, the size distribution of particles was near normal, although the authors acknowledge that particles ranging from sub-micron size to 5 μm could not be accounted for, given the limited resolution of the microscope. Some differences in particle shape were observed for the two regimes. The authors assert that larger particles were produced under the ultrasonic regime due to increased collisions between molten droplets. Some hollow particles were also seen in this analysis.

Given the role of debris, both deliberate and unintended, in various forms of EDM, this study aims to fully characterise the size, shape and distribution of debris produced by EDM at the using SEM for the micro-scale and TEM for the nano-scale. From the information of image processing, a simple debris spark gap can be modelled using the lattice Boltzmann method framework for the solution of Poisson equation, and the influence of typical EDM debris on the relative change in the electric field strength can be determined.

2. Experimental

To generate a high density of EDM debris, TiC and Si electrodes typically used in EDC were set as the negative polarity. Both materials are used normally as donor electrodes which can shed a significant amount of material to the discharge gap. The TiC electrode is manufactured by powder compaction, whereas the Si electrode is a single crystal. The positive electrode work piece was 304 stainless steel. Machining was performed in a small tank containing 60 ml of oil, without externally applied flushing. A cross-sectional area of $100\,mm^2$ was used for all electrodes and machining was stopped after an absolute z-axis translation of 0.5 mm. The electrical parameters used for debris collection tests are shown in Table 1. Electrical parameters used for each electrode type are based on parameters which have been optimised for the electrode to donate the most material to the discharge gap, and there debris collected represents the conditions in which the electrodes would be most used. In order to observe the size and morphology of debris particles, SEM images were collected using a Hitachi S-2600N. TEM images were acquired using a JEOL 2100F at 200 kV. Particle diameters were measured using ImageJ, an open source image processing software. Images of particles were filtered into binary images from which diameters were calculated and plotted using standard statistical analysis methods.

3. Debris imaging

3.1. SEM analysis

EDM was performed at 5 different current settings for each electrode material. Debris was collected and then centrifuged at 14,000 rpm for 90 min, repeated three times using heptane to emulsify and remove the oil before imaging. 5 images of debris for each parameter at a magnification of 2000× were processed to yield particle diameter data. At all currents, for the silicon material, all imaged particles were spherical. For TiC, the vast majority of particles were also spherical except for a small fraction of angular particles. Particles produced using a discharge current of 5.5 A for silicon and 10 A for TiC can be seen in Fig. 1 which were taken using back-scattered electron imaging to enhance elemental contrast. For all debris samples, individual debris particles could be clearly distinguished against the background as bright particles, with a darker matrix of finer debris or oil residue present in the background, likely the lower atomic number element carbon dominating these regions.

Table 1
EDM parameters used to generate debris.

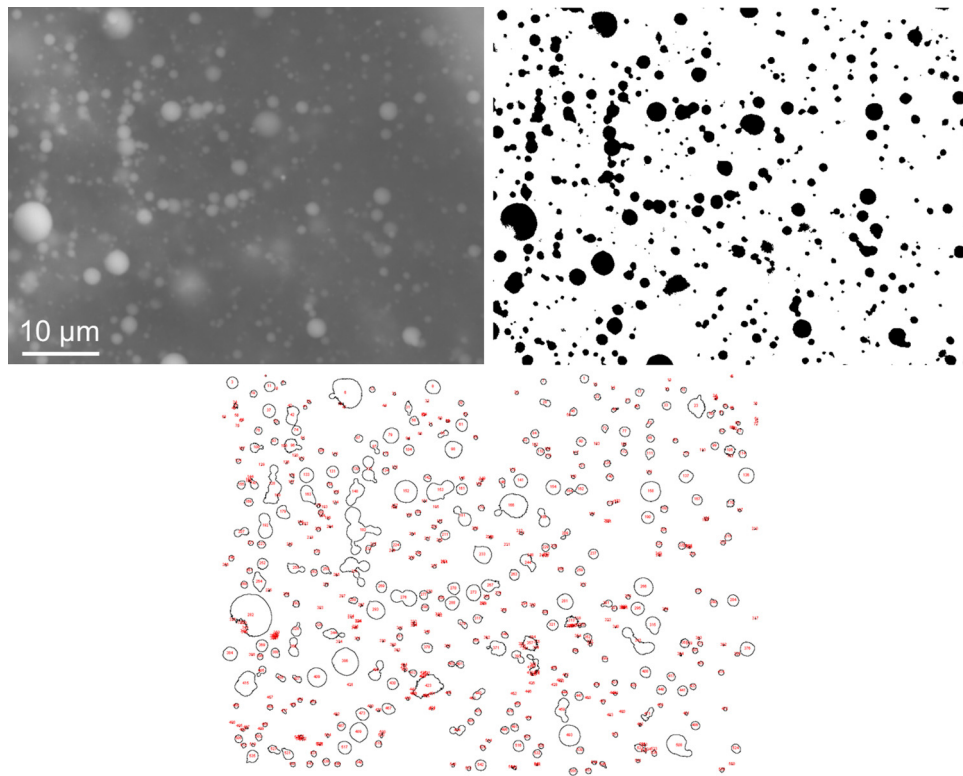|	Si	TiC
Current (A)	4, 4.5, 5, 5.5, 6	8, 9, 10, 11, 12
On-time (μs)	8	8
Off-time (μs)	64	256
Gap voltage (V)	260	320

Fig. 2. Example image processing of an SEM image into a binary image, from which individual particles were identified computationally, and the areas of which were measured.

Fig. 2 shows the image processing procedure used for identifying individual debris particles from the SEM images. The micrographs were first converted into binary images, then individual particles were identified and the area of each was automatically measured. The diameter of each was calculated from the area on the assumption that each was area was circular. Some particles were detected at diameters below 0.2 μm which were clearly not present in the images, and were caused by aberrations in the image processing algorithm, and therefore the counting protocol was instructed to ignore diameters below 0.2 μm.

Histograms which describe the size distribution of particle diameters of parameter 5.5 A for Si and 10 A for TiC are shown in Fig. 3(a) and (b). These distributions are typical of the distributions for each material. Bar charts displaying the mean and median particle sizes are shown in (c) and (d) and show the trend with increasing discharge current. The histograms represent particles above 0.2 μm in size due to the limited resolution of the SEM. This data is essential in order to model debris behaviour and electric field strength. According to Fig. 3, no clear correlation was observed between debris particle diameter and increasing current over the range investigated. The mean particle size of all TiC particles regardless of current was 0.986 μm, 4.1% larger than Si—0.947 μm. The median TiC particle size was 0.738 μm, 10.6% larger than that of Si—0.667 μm. This difference in median size can be seen in the histograms in Fig. 2.

The non-dependence of the debris sizes on current can be attributed to the mechanism by which debris forms during EDM. Schumacher (2004) explains that during discharge, evaporation is thought to be the key mechanism of material removal. However at the end of the discharge duration, the previously overheated molten material at the electrode is ejected in liquid form after which is quickly solidified. Yang et al. (2010) however explain that the evaporated material is removed mainly as atoms and clusters of atoms. So if we assume that the spherical particles seen in the

SEM images were created mainly at the end of discharge, then their properties are not thought to depend directly on the current, but on the rate at which they are ejected and resolidified in the dielectric. For this reason, the particle size distribution is not thought to depend strongly on the discharge current during discharge on-time.

3.2. TEM analysis

Based on the SEM imaging and histogram data of particle sizes measured from the images in section 3.1, the debris contains particles at a smaller scale than can be resolved by SEM. To fully understand the distribution of debris particle sizes created by EDM, TEM imaging was performed. The use of TEM on EDM debris is also useful for clarifying the mechanism of material removal in EDM, for example as predicted by Guo et al. (2014) and Yang et al. (2010), who point out that some of the EDM removal process results in atomic scale debris being produced during the discharge on-time. TEM imaging was therefore performed on centrifuged EDM debris material from both TiC and Si which was left for 24 h in a vacuum chamber for complete evaporation of the heptane liquid.

TEM imaging revealed larger particles up to approximately 1 μm in a matrix of finer debris, an example of which is seen in Fig. 4. The larger spherical particles in Fig. 4 were identified using EDX as containing Ti and C, however given the presence of carbon in the dielectric, it is difficult to say whether the carbon contribution is from the particle itself or from the matrix of debris surrounding it. However it is clear that the large particles originated from the negative polarity TiC electrode. In order to confirm the presence of TiC in the debris imaged by TEM, crystallographic information is required. A selected area electron diffraction (SAD) pattern was taken from a region of fine debris with good electron transparency. The resulting pattern is shown in Fig. 4(b), with the location shown in (a). Although the rings, indicative of a polycrystalline structure dominate the pattern, some blurring of the signal can be seen, sug-
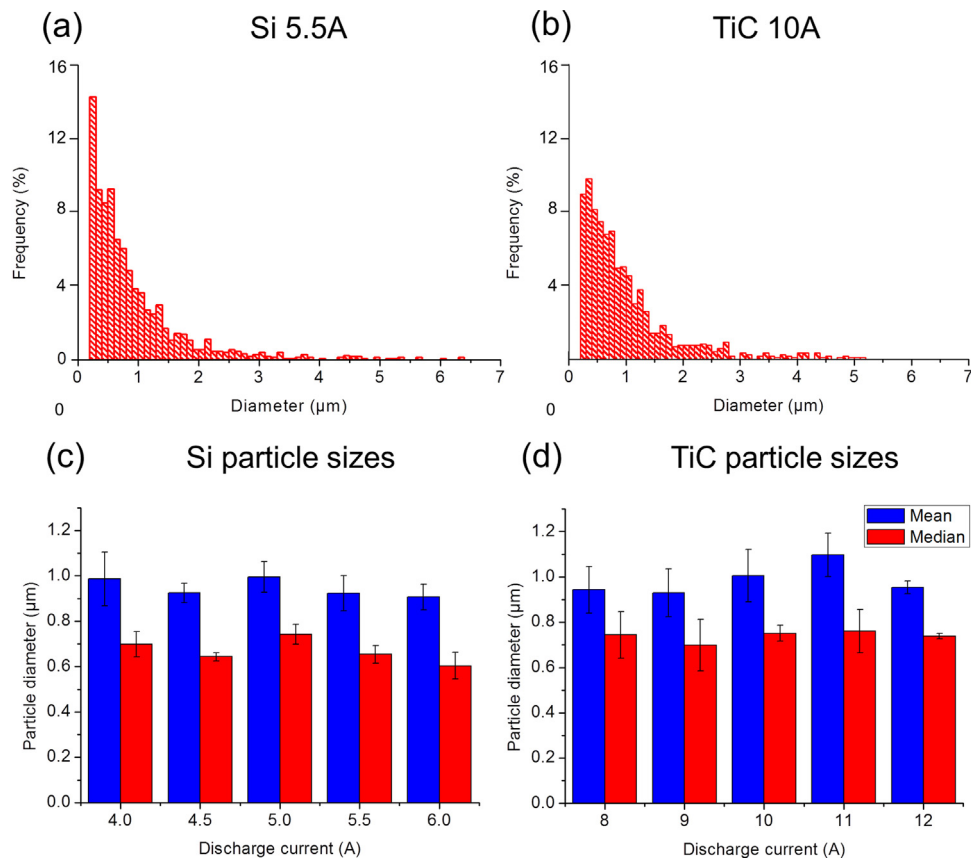
Fig. 3. Histograms of particle diameters of (a) Si at 5.5 A and (b) TiC at 10 A, and average particle sizes. Error bars represent the standard deviations of the results of the 5 images used to calculate the average values.

gesting the presence of some amorphous phase. The XRD pattern taken from the original TiC electrode material is overlaid with the rings in Fig. 4(b), indicating the same D-spacing was measured *via* electron diffraction. This is strong evidence that the matrix of debris surrounding the larger micron-scale particles is dominated by extremely small debris particles from the electrode.

EDX analysis was performed on both the Si and TiC samples at high magnification, where particles were typically less than 10 nm diameter. EDX mapping and quantification of silicon debris is shown in Fig. 5. In the dark-field image, particles down to 1 nm can be seen. The STEM image was taken in high-angle mode, in which elements with a high atomic number give brighter signals. Elemen-

tal analysis confirmed that even at this scale, silicon is prevalent and well distributed in the field of debris, and the distribution of silicon fits with the brighter contrast particles seen in the STEM image. Carbon from the oil is however the most dominant element in the region. Iron from the steel workpiece was also detected and its map location corresponds to the brightest regions of the STEM image. EDX analysis performed on the TiC debris, also revealed a small amount of iron was present, although carbon was again the most dominant element, followed by titanium. The titanium was also well distributed through the debris.

TEM images of TiC and Si debris are shown in Fig. 6. Both samples revealed debris particles at both limits of the TEM resolution—down
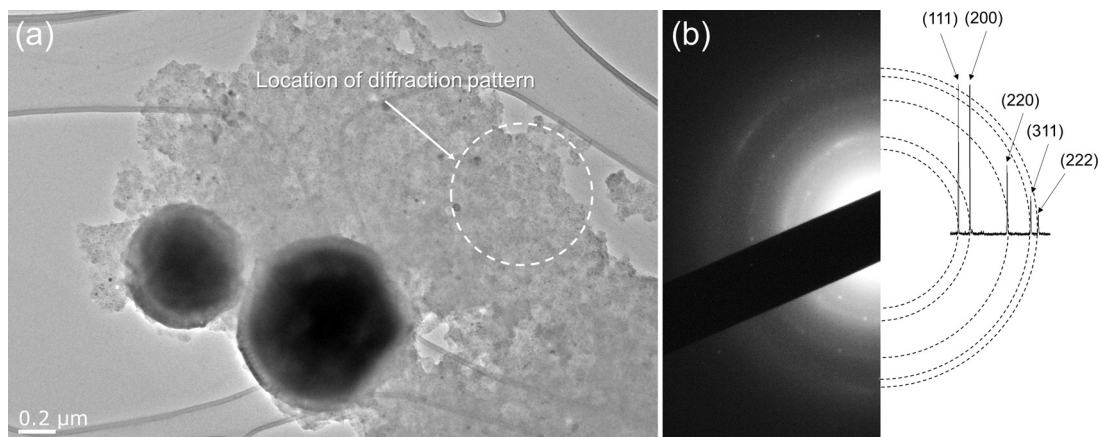

Fig. 4. (a) Bright-field TEM image of TiC particles in a matrix of smaller debris. In (b) the electron diffraction pattern confirms that crystalline TiC dominates the field of debris. The XRD pattern from the TiC electrode is overlaid with the electron diffraction pattern.
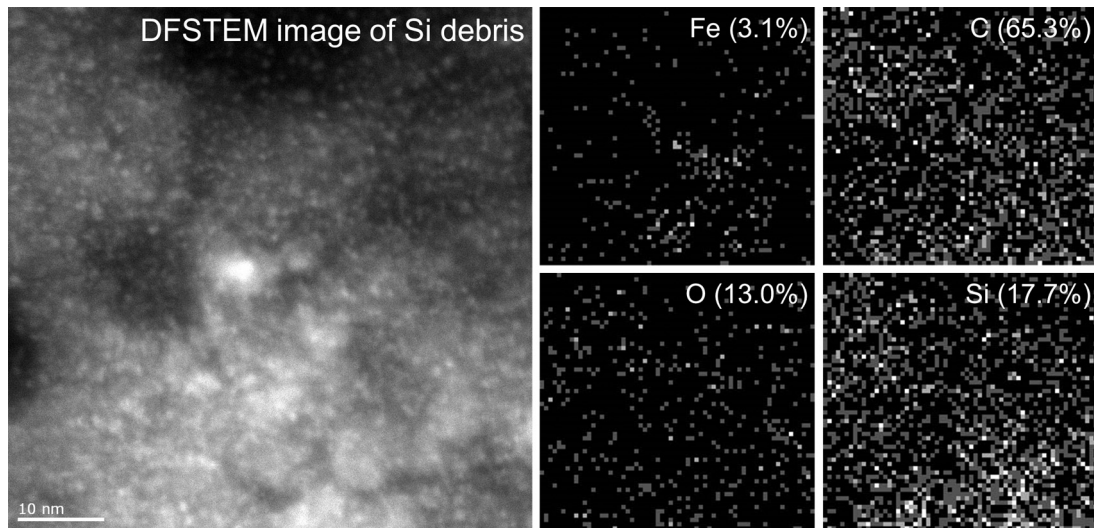
Fig. 5. Dark-field STEM image of Si debris and EDX mapping of imaged region.

to approximately 1 nm and up to several μm diameters, corresponding to the largest field of view possible with this instrument. In Fig. 6(a) the lattice fringes of a 5 nm TiC particle can be seen, inferring that it is a single crystal. Silicon particles observed were exclusively spherical throughout the size distribution, whereas for TiC, there were numerous particles of angular shapes, for example as in Fig. 6(b), although the majority were spherical. This can be explained by the structure of the electrode materials which were the source of the debris. The TiC electrode was fabricated *via* a powder compaction method, and therefore some of the debris collected was likely mechanically pulled out by discharge due to the material's weak bonding strength and released not by direct melting as is expected to be the case with Si electrode. Therefore the size distribution of the TiC debris is not entirely dependent on the discharge parameters but also on the material and precondition of the electrode. The characteristic of the electrode to shed material in its original sintered form, as well as have it ejected by discharges may in part explain the slight difference in morphology between the Si

and TiC debris. However the material condition does not appear to affect the size of particles at the nano-scale.

Interestingly, in both samples of debris, particles at vastly different size ranges were observed. Although in both samples, there were many spherical particles between approximately 100 nm and 2 μm, much of the debris was observed to be several nm in diameter, with possibly sub-nm particles existing which could not be detected. The prevalence of these extremely small particles mixed with much larger particles may support the simulation results by Yang et al. (2010) which suggests that two mechanisms are responsible for material removal by EDM: vaporisation and bubble explosion, the first of which is expected to yield debris as single atoms or small clusters of atoms. Images such as Figs. 6(c) and 5(a) contain electrode debris particles of relatively uniform size indicative of this vaporisation mechanism. Guo et al. (2014) explain that the expulsion of single atoms and clusters of atoms occurs after the initial thermal shock of discharge, resulting in stress in the material, subsequently causing the release of larger particles of debris.
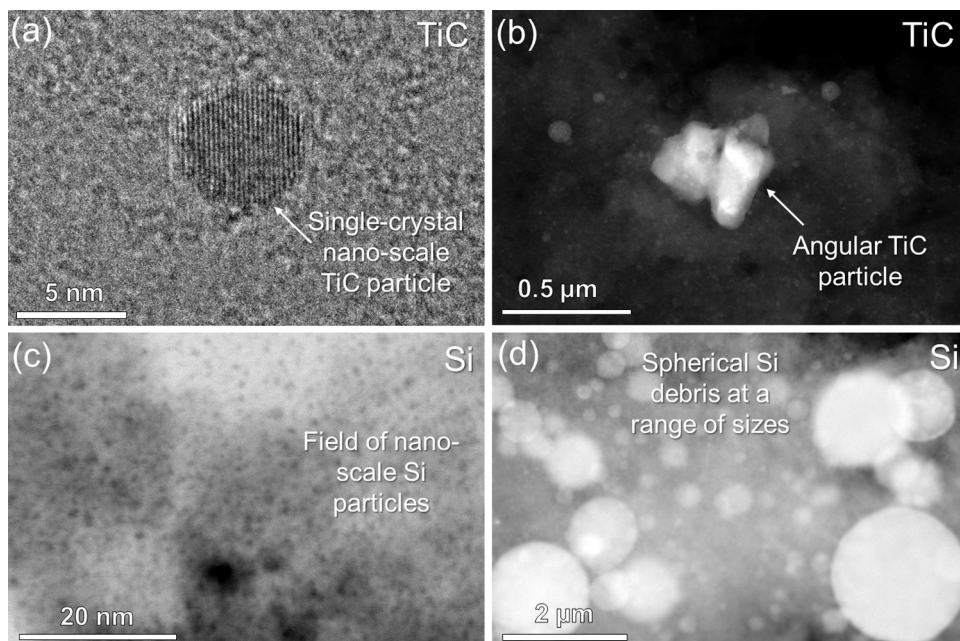

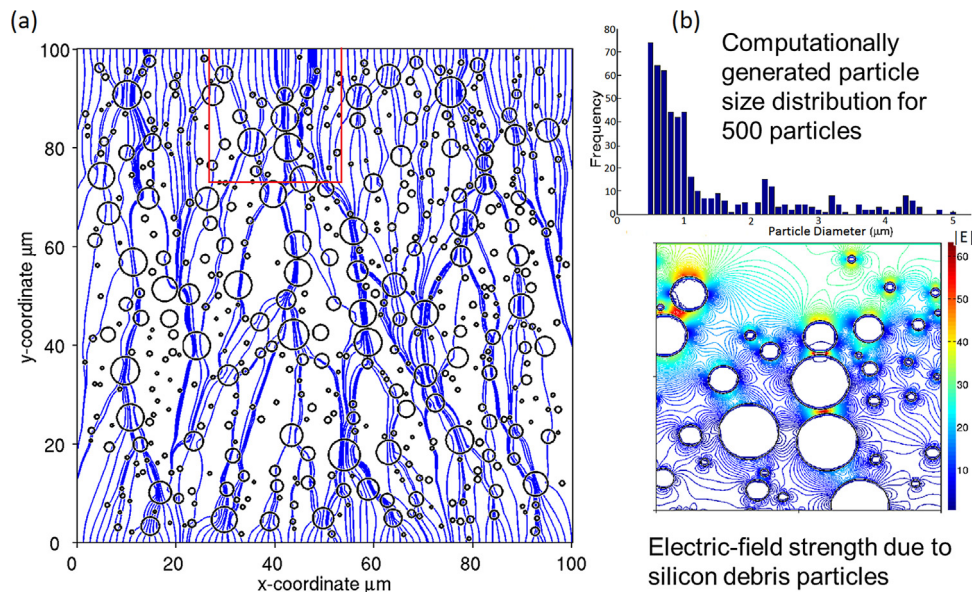**Fig. 6.** Compilation of TEM images of Si and TiC at various magnifications.

Fig. 7. Lattice Boltzmann computations for potential-field with silicon debris in dielectric: (a) streamlines of electric-field E = −Ñf, (b) particle size distribution used in this model and local variation of magnitude of electric field around few debris.

Based on these simulation studies, the smallest particles observed by TEM in this work are likely associated with material removal taking place by vaporisation during discharge on-time. The much larger particles observed by SEM are likely to have been created either at the very beginning of discharge *via* the initial thermal shock effect proposed by Guo et al. (2014) which occurs within a few picoseconds after discharge begins, or they were created by the more conventional theory of the pressure drop at the end of discharge duration causing expulsion of molten material. However the cause of material removal, these results add weight to the theory of multiple different removal regimes occurring at different stages of discharge.

4. Lattice-Boltzmann modelling of spark gap

Data collected from debris experimentation was used in conjunction with a kinetic theory based lattice Boltzmann (LB) framework to analyse debris particle behaviour in the pre-spark gap. The LB method is an emerging multi-physics fluid flow solver which is compatible with parallel computing on CPU and GPU computers (Guo and Shu, 2013). The LB framework has been used to efficiently solve the variable coefficient Poisson equations with pseudo-time iterations on single as well as multiple grid levels (Patil et al., 2014). In this case a novel LB framework was used to compute the electric potential field values and maximum strength of an electric field in the presence of debris and in the two-dimensional domain of size $(100\,\mu m \times 100\,\mu m)$, thus allowing the fundamental influence on realistic debris sizes on the likelihood of EDM discharge to be understood. The debris particles (solid phase) and dielectric (fluid phase) have distinct electrical conductivities which pose few numerical difficulties to this modelling method. Consistent with experimental results, two types of debris material, Si and TiC are explored here. It should be noted that for a complete, absolute picture of the electric conditions of the gap in typical conditions, the influence of the workpiece material debris, in this case steel, should be considered. As seen in Fig. 5, however, only 3.1% by weight of the area analysed consisted of iron. Therefore the only the primary constituents of the gap were considered for the purposes of this model. The conductivity values considered are sf = 1 × 10 − 5 S/m, sSi = 1 × 10 − 3 S/m and sTiC = 1 × 10 − 2 S/m,

however, these are easily varied for alternate electrode materials. The computational domain is discretised in a regular square grid of 1000×1000 lattice node points. Thus, with 5 lattice node points along the diameter of the randomly located smallest debris particle it is possible to approximate the experimentally observed smallest debris size of $0.5\,\mu m$. Computation of particle sizes below $0.5\,\mu m$ is not possible in the current work, and therefore the particle size data generated from SEM imaging, as in Fig. 3 were used in the simulation.

A plot depicting a converged electric field for silicon debris having volume fraction of 0.12 is shown in Fig. 7(a), with an enlarged view in (b) to illustrate electric field (magnitude) variation around a few debris particles. Clearly large debris particles dominate the electric field concentrations, despite the higher frequency of smaller particles as seen in the histogram in Fig. 7. This effect could significantly reduce the breakdown voltage of the gap.

Using this methodology it is now possible to predict the electric field strength as a function of debris concentration within the gap. The variation of the normalized value of maximum strength of an electric-field in the domain is plotted with respect to the concentration of TiC and Si debris particles in the spark gap in Fig. 8. The magnitude of uniform electric-field strength corresponding to the clean oil is considered as the normalising value.
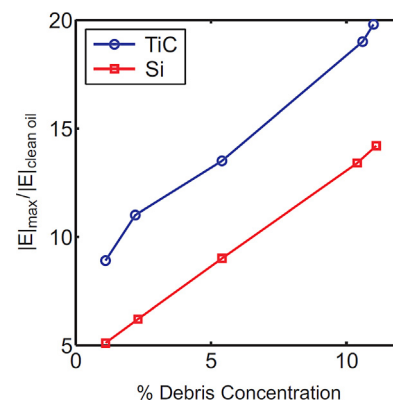

Fig. 8. Variation of normalized value of maximum electric-field strength with respect to debris particle (volume) concentration.

It is shown in Fig. 8 that the maximum of |E| in the domain increases almost linearly with respect to the percentage volume fractions of particles (from 1.1% to 10.6%). Interestingly, the last data point on the graph at 11%, despite only a marginal increase in the volume fraction 10.6%, represents a significantly larger absolute number of particles (over 900 compared to 500). This increase also caused only a marginal increase in electric field strength ratio. The TiC debris results in a larger increase in the electric field strength than the Si debris at the same concentration due to its larger conductivity. Based on these results, it is clear that even the simple presence of debris can yield a significant increase in maximum electric field strength (a five-fold increase with only a 1.1% volume fraction for Si and more than eight-fold for TiC), and there is a rapid increase in the field strength ratio with an increasing volume fraction (an almost twenty-fold increase in field strength ratio with 11% volume fraction of TiC). These results provide a basis for determining the optimum level of flushing in the gap in the case of deliberate addition of debris for enhancement of machining or for coating. The results also underline the importance of considering flushing of the discharge gap during EDM in order to avoid extreme sparking conditions (arcing). By understanding the increase in electric field strength in the machining gap in EDM, it is also possible to predict the increase in gap size that can be used to guide the servo control in EDM. The composition of the debris particle in the gap has also been shown as a critical parameter in terms of electric field concentration, and should therefore also be considered if gap conditions are to be precisely controlled.

5. Conclusions

- In this study debris formed as a side effect of electrical discharge machining was imaged using TEM and SEM, revealing particle sizes as small as 1 nm and possible lower and as large as approximately 10 μm. Elemental analysis and electron diffraction confirmed that debris from both electrodes is present at all scales of imaging. The extreme range of sizes is indicative of a complex removal process which includes vaporisation as well as expulsion due to bubble explosion or pressure drop.
- Electrode debris particles were present in all regions of the samples imaged by TEM, adding evidence that debris does in fact play a key role in the electrical conditions in the discharge gap.
- Debris size showed no clear dependence on discharge current.
- The morphology of solidified debris particles is largely spherical even at the lower end of the size distribution as observed by TEM. This is typical of rapidly cooled metals as a result of surface tension effects. Some TiC debris was angular, likely due to it being ejected directly in the solid form from the powder sintered electrode.

- Image processing was used to determine debris size distributions which were used to inform an electric field model based on a lattice Boltzmann framework. The magnitude and variation of the relative increase in electric field strength was determined against volume fraction of particles. Up to an approximate 20 times increase in relative maximum electric field strength was calculated for an 11% volume fraction of TiC. For silicon particles the relative electric field maximum was less for all volume fractions. Interestingly, even with a 1.1% volume fraction of particles for both materials, the maximum electric field strength is significantly increased.

References

Chow, H.-M., Yang, L.-D., Lin, C.-T., Chen, Y.-F., 2008. The use of SiC powder in water as dielectric for micro-slit EDM machining. J. Mater. Process. Technol. 195, 160–170.

Gatto, A., Bassoli, E., Denti, L., Iuliano, L., 2013. Bridges of debris in the EDD process: going beyond the thermo-electrical model. J. Mater. Process. Technol. 213, 349–360.

Guo, J., Zhang, G., Huang, Y., Ming, W., Liu, M., Huang, H., 2014. Investigation of the removing process of cathode material in micro-EDM using an atomistic–continuum model. Appl. Surf. Sci. 315, 323–336.

Guo, Z., Shu, C., 2013. Lattice Boltzmann Method and Its Applications in Engineering. World Scientific.

Kansal, H.K., Singh, S., Kumar, P., 2007. Effect of silicon powder mixed EDM on machining rate of AISI D2 die steel. J. Manuf. Processes 9, 13–22.

Luo, Y.F., 1997. The dependence of interspace discharge transitivity upon the gap debris in precision electrodischarge machining. J. Mater. Process. Technol. 68, 121–131.

Murti, V.S.R., Philip, P.K., 1987. An analysis of the debris in ultrasonic-assisted electrical discharge machining. Wear 117, 241–250.

Patil, D.V., Premnath, K.N., Banerjee, S., 2014. Multigrid lattice Boltzmann method for accelerated solution of elliptic equations. J. Comput. Phys. 265, 172–194.

Peças, P., Henriques, E., 2003. Influence of silicon powder-mixed dielectric on conventional electrical discharge machining. Int. J. Mach. Tools Manuf. 43, 1465–1471.

Schumacher, B.M., 2004. After 60 years of EDM the discharge process remains still disputed. J. Mater. Process. Technol. 149, 376–381.

Tosello, G., Bissacco, G., Tang, P.T., Hansen, H.N., Nielsen, P.C., 2008. High aspect ratio micro tool manufacturing for polymer replication using μeDM of silicon, selective etching and electroforming. Microsyst. Technol. 14, 1757–1764.

Yang, X., Guo, J., Chen, X., Kunieda, M., 2010. Molecular dynamics simulation of the material removal mechanism in micro-EDM. Precis. Eng. 35, 51–57.